Development, Validation, and Performance Evaluation of An Air-Driven Free-Piston Linear Expander Numerical Model

Ahmed T. Raheem
Center for Automotive Research and Electric Mobility (CAREM), Universiti Teknologi PETRONAS

A. Rashid A. Aziz
Center for Automotive Research and Electric Mobility (CAREM), Universiti Teknologi PETRONAS

Saiful A. Zulkifli
Center for Automotive Research and Electric Mobility (CAREM), Universiti Teknologi PETRONAS

Abdalrazak T. Rahem
Department of Electrical, Electronic and System Engineering, Faculty of Engineering

他

https://doi.org/10.5109/4774218

出版情報：Evergreen. 9 (1), pp.72-85, 2022-03. Transdisciplinary Research and Education Center for Green Technologies, Kyushu University
バージョン：

Development, Validation, and Performance Evaluation of An Air-Driven Free-Piston Linear Expander Numerical Model

Ahmed T. Raheem[1,2*], A. Rashid A. Aziz[1,2*], Saiful A. Zulkifli[1,3], Abdalrazak T. Rahem[4], and Wasiu B Ayandotun[1,2]

[1]Center for Automotive Research and Electric Mobility (CAREM), Universiti Teknologi PETRONAS, 32610 Seri Iskandar, Perak, Malaysia.

[2]Department of Mechanical Engineering, Universiti Teknologi PETRONAS, 32610 Seri Iskandar, Perak, Mal aysia.

[3]Department of Electrical & Electronics Engineering, Universiti Teknologi PETRONAS, 32610 Seri Iskandar, Perak, Malaysia

[4]Department of Electrical, Electronic and System Engineering, Faculty of Engineering, 43600 UKM, 43600 Bangi, Selangor, Malaysia.

*Correspondence: rashid@utp.edu.my; a.t.utp3@gmail.com

(Received September 3, 2021; Revised February 24, 2022; accepted February 24, 2022).

Abstract: The free piston linear expander (FPLE) is an energy conversion device that converts mechanical energy into electric energy by using a linear electric machine (LEM) without emission. This research addresses the numerical modeling of a dual-piston air-driven FPLE constructed on the basis of the free piston engine linear generator (FPELG) concept. The model was built in MATLAB/Simulink. The simulation results were in good agreement with the experimental data. Where the in-cylinder pressure and displacement profiles attained errors of less than 10% (within the acceptable range). Then, the predicted results of the simulation model, namely, the displacement profile, in-cylinder pressure, piston velocity, and engine power results were analyzed. Findings indicate that intake pressure was the most important parameter for enhancing engine performance. The in-cylinder pressure increased by approximately 16% and 21.7% when the intake pressure was increased from 5 to 6 bar and from 6 to 7 bar, respectively. The piston velocity increased by approximately 12.3% when the intake pressure increased by 1 bar. Finally, engine power increased by approximately 26.5% and 30.6% when the intake pressure increased from 5 to 6 bar and from 6 to 7 bar, respectively.

Keywords: free piston linear expander; numerical model; engine performance

1. Introduction

Wide attention has been devoted by researchers to the development of alternatives to conventional internal combustion engines (ICEs). In addition, researchers have focused on the production of new-generation engines with low emission, high performance, and enhanced stability. In order to decrease the exhaust gasses emission some researchers focused on renewable energy such as wind and sunlight. The Savonius wind turbine was considered one of the most important clean energy with low cost[1)]. Al-Ghriybah et al.[2)] studied the influence of the inner blade position on the performance of the Savonius rotor. Moreover, to improve the power output, the influence of spacing between inner blades on performance was investigated[1)]. While some other researchers used electric engines as an alternative of the conventional engine to decrease the mission. For example, the motorcycle using an electric engine was designed and studied[3)]. The free-piston engine linear generator (FPELG) is considered to be one of the alternative converter technologies suitable for many applications e.g., hybrid vehicles, power plants, and hydraulic tools[4,5,6)].

The first concept of FPE was reported by Pescara in the 1920s[7,8)]. The components of FPELG can be described according to two main parts: the linear electric machine (LEM) and the free-piston engine (FPE)[9,10,11)]. FPELG has some specifications such as low emission, and high thermal efficiency, also the FPELG uses fewer components to ensure lesser friction compared with conventional engines[4,5,6,12)]. The pistons move freely between the dead centers because the FPELG does not have a crankshaft[6,11,12)]. Thus, the FPELG entails both advantages and disadvantages.

For the advantages, the FPELG produces lesser friction compared with conventional engines, as only the friction between the cylinder's walls and piston ring (piston assembly) acts as the main friction, and the other forces emanating from the piston skirt, accessories, and bearing are negligible[5,6,10,13]. In addition, multi-fuel engine, low emission, and high thermal efficiency[4,5,6,12]. While for the disadvantage, the FPELG suffers from a number of technical issues, including poor control of piston motion[14,15,16]. In addition, as the crankshaft is lacking in FPELGs, free movement is produced for the pistons between the dead centers, namely, the top dead center (TDC) and the bottom dead center (BDC)[6,11,12]. Thus, the pistons can only be controlled by the forces emanating from the pressure gas in the cylinders and load[12,17,18]. Consequently, cycle-to-cycle is produced which is considered one of the main issues of the FPELG[6,12,18,19]. Such issues pertaining to the operation and high performance remain unresolved, thus preventing the commercial production of FPELG. In addition to the aforementioned initiatives, researchers have developed FPELG models and implemented simulations on the basis of simplified conventional engine models. However, this approach is unsuitable, indicating the need for further investigation and development of new models.

In general, linear FPEs can be classified into four main types, as shown in Figure 1.

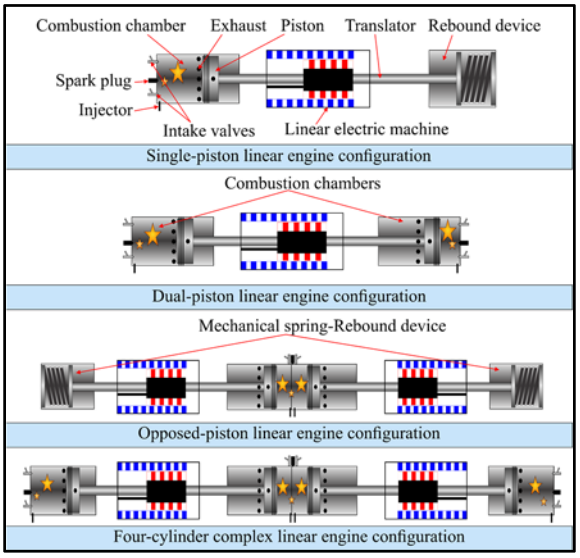

Fig. 1: T Types of linear FPE configuration

The first type is a single-piston FPE[9,18,20] this kind of FPELG has a simple mechanical specification with high controllability[6,21]. The second type is the double-piston FPE[22,23] can be described the components by LEM connected between two combustion cylinders and no-rebound device is present[6,12]. The advantages of double piston FPE compared to other types are a high compression ratio is produced and higher power to weight ratio with a more compact device are also involved[24]. While the disadvantages of double piston FPE can be summarized as lesser controllability of the piston motion compared to the single-piston type, thus, cycle-to-cycle variations are produced[14,25]. Third type is the opposite-piston FPE[26], the components include one combustion chamber with two opposed piston units connected with two LEM and two rebound device. The losses of heat are low by using a shared combustion chamber compared to other types of FPE. The engine size of the opposite-piston type is bigger compared to the single and dual piston FPE types[5,6,26,27]. Last main type is the four-pistons FPE. Among them, the combination between opposed-piston and dual-piston types are the complex ones[5,6,28].

Zhao et al.[29] developed a hydraulic FPELG. Their operating principle was actuated by converting the energy originating from the chemical reaction of air and fuel to hydraulic energy. In their study, the dynamic combustion and hydraulic characteristics of the hydraulic FPELG were investigated. Meanwhile, as the duration time of the compression stroke is longer than that of the expansion stroke, the dynamic behavior with respect to the hydraulic FPELG is asymmetric. Hu et al.[30] studied the behavior of a hydraulic FPELG and found that the premixed combustion phase could produce combustion with a shorter duration than the normal combustion.

Abidin et al.[31] developed a dual-piston configuration of the FPELG. The operating principles of FPELG for the starting stage was studied. The motoring force was utilized to push the piston between the TDC and BDC in the starting stage. The motoring force was used to increase the piston velocity gradually until a combustion force was reached, thus starting a combustion. However, the combustion pressure was influenced by the capacity of the battery, which was used to control the piston's motion. In another research[32], motoring forces were used for the starting stage of the FPELG. The process was continued until the combustion force was achieved, and then the system was switched into the combustion process. Results showed that the combustion started after four cycles, and a starting force of 125 N was achieved. Another study Zhu et al.[33] used a hydraulic damper in the opposite piston configuration of the FPELG to produce a resonance movement. Certain limitations were observed in the piston motion control, suggesting the need for a control system with more complex configurations. Can be concluded that difficulties in the starting operation of FPELG is existing. A control strategy to improve the starting operation of FPELG is required to overcome the issues related to the starting stage.

The air-driven FPLE can be easily described by referring to the bounce chamber (rebound device) on both sides of the engine. A linear motor, mechanical spring or cylinder for the gas spring was used as a rebound device[4,5,12]. The FPELG with a spring as a rebound device was developed. The spark-ignition (SI) FPELG with a homogeneous charge compression ignition (HCCI) was investigated. Results showed that the intake pressure and compression pressure could be adjusted by manipulating

the spring's stiffness. Thus, the tendency of the piston to hit the head of the cylinder and engine knocking were both avoided[28]. While gas spring was used as a rebound device in FPELG by Mikalsen and Roskilly[16]. Moreover, two bounce chambers were used to reduce the pressure leakage. Results showed that the engine could run for approximately 4 hours without cooling and lubrication problems[11].

The numerical model of FPELG by using a bounce chamber as a rebound device was proposed. Motoring force was used in the starting stage to run the FPELG[34]. A low compression ratio was derived because of the limited starting force of the motoring device. Sandia National Laboratories[35] developed an FPELG model that comprised dynamic and thermodynamic sub-models. A research group in West Virginia University[36] also developed an FPELG numerical model to investigate certain combustion characteristics. However, both studies focused on the thermodynamic and combustion directions of FPELGs. In another study, the numerical modeling and simulation were conducted using MATLAB/Simulink for the opposite-type FPELG[27]. Results showed that the model could predict in-cylinder pressure with good accuracy. Other researchers[37,38] investigated the performance and piston motion of the single-piston FPELG via numerical modeling to demonstrate the effect of spring stiffness on engine frequency. Jia et al.[10] developed a numerical model for both the starting stage and steady-state operating stage of an FPELG. In another study, the optimum operating condition during the cold start-up stage of an engine was studied using a model established in MATLAB/Simulink[39]. However, a model based on the dual-piston FPELG was particularly established. The literature review indicates that a majority researchers have focused on the combustion direction of the FPELG, whereas only a few of them studied the FPELG, including the rebound device.

On the other side, many researchers in different countries are presently pushing vehicle-manufacturing companies and power plants to apply the emission reduction rules as a means of reducing the gas emissions responsible for global warming[20,40,41]. Consequently, the studies pertaining to alternative fuels with low emissions, such as hydrogen fuels and biofuels, have also increased[18,20,40,42]. The effect of hydrogen on ICEs was also studied[43]. Findings showed that peak pressure could be increased, to enhance the efficiency of the engine. Emission gases (i.e., CO2, HC, and NOx) from hydrogen fuel were lesser compared with the fuel without H2. Another study demonstrated that the FPELG with a four-stroke cycle has a higher thermal efficiency (approximately 13.2%) compared with that with a two-stroke cycle[19]. However, it was produced more NOx emissions. Huang and Kong[44] studied the influence of adding hydrogen to a fuel mixture (i.e., methane–air mixture) with different equivalence ratios. A number of studies[4,5,6,12,15] showed that the power-to-weight ratio can reach high values for the dual-piston FPELG compared with those of the other types, but its energy conversion efficiency is low because of poor piston motion control and combustion and generator issues. In addition, the low-efficiency issue can be attributed to gas leakage and excessive heat transfer, among others[15,45].

For the conventional engines, the relevant literature can be summarized as follows. The performance of the four-stroke engine of the CNGDI type and different injection positions were studied. Researchers found that start injection timing has a significant impact on brake torque, volumetric efficiency, and brake thermal efficiency[46]. Another study found that the power generator could be developed on the basis of the organic rankine cycle (ORC) system. The thermal efficiency was between 2.5% and 4.45%, and the expander rotation was between 1650 and 2750 rpm[47]. Other researchers focused on the optimization of the spark-ignition engine. In this scheme, the gasoline fuel blend was used by varying the amount of octane while maintaining a specific volume of bioethanol. The test involved an injection duration of less than 10% and advanced ignition timing. This setup allowed for the collection of data pertaining to optimization. The researchers found that some parameters could be improved (engine power, torque, and specific fuel consumption) based on the control strategy[48]. However, the response surface methodology (RSM) was one of the most important tools for optimizing certain parameters of the engine[9,49]. This scenario implies that, on the one hand, the FPELG remains far from being commercially applicable. On the other hand, emission should be continuously considered as one of the most important challenges for all types of ICEs.

In conclusion, the air-driven FPLE is one of the important technologies for converting mechanical energy into electric power without any emissions involved. The engine performance is one of the most critical issues of the FPLE engine. However, to the best of our knowledge, no research pertaining to the influence of the operating parameters such as intake pressure on the FPLE performance has been conducted. Moreover, only a few studies in the literature have been experimentally investigated of the FPLEs. In addition, models to describe FPLE engines that can operate with only two air-driven cylinders are not found in the literature. Therefore, the objective of this study is to explore the influence of the operating parameters on FPLE performance. The numerical model of the FPLE with air-driven cylinders is proposed. The simulation model is established using MATLAB/Simulink, and then the simulation result is validated by experimental data. The error is less than 10% for the peak pressure. Thus, the predicted results of the model are in good agreement with the experimental data. Furthermore, this study investigates the influence of intake pressure on displacement profile, in-cylinder pressure, piston velocity, and engine power. The results show that intake pressure has a significant effect on engine

performance. When the intake pressure is increased, the in-cylinder pressure, piston velocity, and engine power also increase. FPLE performance can be improved by increasing the intake pressure. Further study is required to explore this topic on optimal intake pressure.

2. Numerical modeling and simulation of FPLE

2.1 Dynamic modeling of FPLE

The dynamic modeling of the FPLE is derived based on Newton's second law. Furthermore, the FPLE system can be demonstrated on the basis of the FPELG's operating principle. When the engine is running, two forces act on the piston assembly, one for each cylinder. These forces originate from the gas pressure that is compressed during the FPELG's operation. The forces work alternately to guarantee a resonance movement, i.e., pushing the piston between TDC and BDC. Figure 2 shows the free-body diagram of the air-driven FPLE and the corresponding forces. Thus, the dynamic equations can be expressed as.

$$m\frac{d_x^2}{dt^2} = F_l(t) - F_r(t) - F_{LEM}(t) - F_f, \quad (1)$$

where m (unit: kg) represents the mover assembly mass, x (m) represents the position of piston, t (s) represents time, F_l (N) represents the force acting on piston in left cylinder, F_r (N) represents the force acting on the piston in the right cylinder, F_f (N) represents the friction force, and F_{LEM} (N) represents the LEM force.

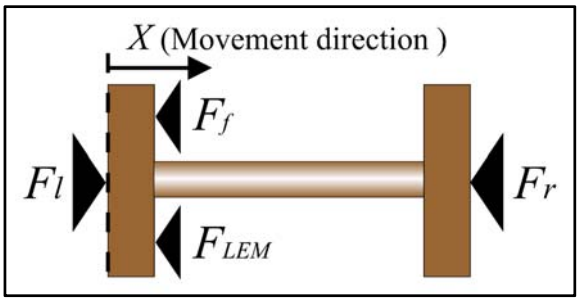

Fig. 2: Free body diagram of the air-driven FPLE

2.1.1 Modeling of the air-driven expander

The air-driven expander equations are derived using the ideal gas concept. On the other hand, the operation process of the air-driven expander is similar to the ICE, but it does not entail a combustion process (i.e., no ignition and fuel injection systems)[50]. Thus, the modeling can also be derived based on the ideal gas equations or combustion chamber equations by removing the formulas related to the combustion process. Figure 3 shows the pressure–volume (P-V) diagram of a trapped gas; this scheme is used as the basis for calculating the energy conversion. Thus, the stored energy during engine operating can be calculated using Equation (2).

$$E_s = \int_{V_B}^{V_T} (P_{ins} - P_0)\ dV, \quad (2)$$

where E_s is the stored energy (J), V_T is the instantaneous volume when the piston's position is at TDC (m^3), V_B is the instantaneous volume when the piston's position is at BDC (m^3), P_{ins} is the instantaneous gas pressure in the cylinder (bar), P_0 is the initial gas pressure in the cylinder (bar), and V is the instantaneous working volume. While the compression energy can be expressed as

$$E_c = \int_{V_1}^{V_2} P\ dV, \quad (3)$$

where E_c is the energy of compression (J), and P is the in-cylinder gas pressure.

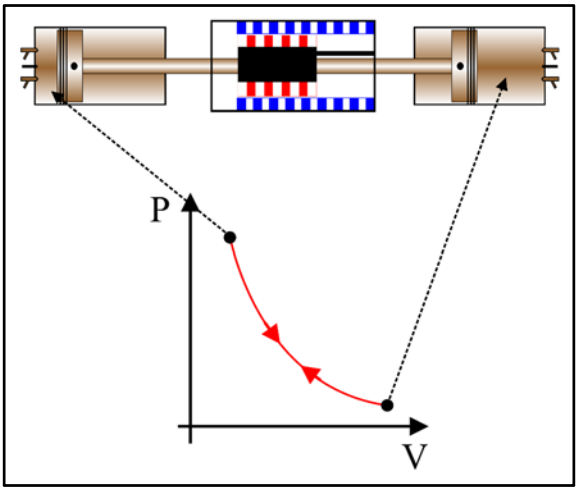

Fig. 3: P-V diagram of the trapped gas

Figure 4 shows the air-driven cylinder parameters used in the numerical model. In addition, the trapped gas pressure model, including the change rate of the temperature, can be described using the ideal gas concept, which is given by

$$P \times V^{\gamma} = C, \quad (4)$$

where C is a constant, and γ is the polytropic exponent.

The Equation after differentiating with respect to time can be written as

$$V^{\gamma} \times \frac{dP}{dt} + \gamma \times P \times V^{\gamma-1} \times \frac{dV}{dt} = 0 \quad (5)$$

Assuming that Equation (5) is a function of temperature, the final equation for calculating the change rate of the gas pressure in the right cylinder is

$$\frac{dP_r}{dt} = \frac{1}{V}\left[(\gamma-1)\left(\mu_{inj}\frac{dm_{inj}}{dt} - \mu_{ex}\frac{dm_{ex}}{dt} - \rho A_T(T-T_w)\right) - \gamma P_l \frac{dV}{dt}\right], \quad (6)$$

where the P_r is the gas pressure in the right cylinder, μ_{inj} is the injected mass enthalpy, μ_{ex} is the exhausted mass enthalpy, m_{inj} is the mass of injected gas, m_{ex} is the mass of exhausted gas, ρ is the heat transfer coefficient, A_T is the total area of heat transfer, T is the temperature of the chamber, and T_w is the temperature of cylinder wall.

V is calculated as

$$V = \pi\frac{D_b^2}{4}(h_m + x), \quad (7)$$

where h_m (m) is the minimum distance (the distance from TDC to the head of the cylinder), x (m) is the instantaneous piston displacement, and D_b (m) is the cylinder's bore diameter.

A_T is calculated as

$$A_T = \pi D_b(h_m + x) + 2\left[\pi\frac{D_b^2}{4}\right] \quad (8)$$

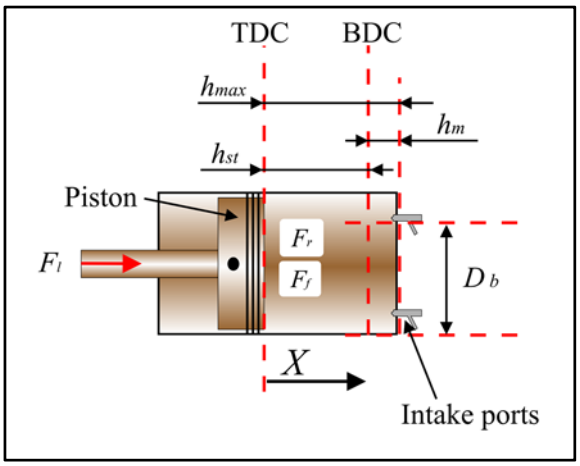

Fig. 4: Parameters of the air-driven cylinder

2.1.2 LEM modeling

The LEM in some FPELG works with two stages i.e., motoring mode and generating mode. While in some other FPELG the LEM works as only in generating mode[12]. However, in this study, the LEM only works as a generator. In order to represent load, assume that a resistor is provided to the system. Figure 5 shows the circuit used in the proposed LEM model in this study. Faraday's law was considered in the LEM modeling.

Faraday's law is given by

$$e = \frac{Nd\Phi}{dt}, \quad (9)$$

where N represents coil turns number, Φ represent the flux, and e represents the induced voltage.

On the basis of a phase-equivalent circuit model and assuming that the Equation is a function to time, the current and the induced voltage can be expressed as

$$\varepsilon(t) = (R_p + R_l)I(t) + L\frac{d}{dt}I(t) \quad (10)$$

$$I(t) = \frac{\varepsilon(t)}{R_p + R_l}\left(1 - exp^{-\frac{1}{R_p+R_l}t}\right), \quad (11)$$

$$\varepsilon(t) = \Phi N L_c M_{th}\frac{\varphi}{2\tau}sin\left(\frac{\pi x}{\tau}\right)\frac{dx}{dt}, \quad (12)$$

where I represent the instantaneous current, ε represents the instantaneous voltage, R_p represents the phase-winding resistance, R_l represents the load resistance, M_{th} represents the PM thickness, L_c represents the coil length that cuts the magnetic lines, x represents the piston displacement, and φ represents the vacuum permeability.

From Equations (11) and (12), the total electromagnetic force can be written as

$$F_{LEM} = 6L_c^2N^2g_{max}^2\frac{1}{R_p + R_l}\left(1 - exp^{-\frac{R_p+R_l}{L}t}\right)\frac{dx}{dt}, \quad (13)$$

where g_{max} represents the maximum air gap flux density that can be calculated as

$$g_{max} = \frac{4\varphi}{\pi g_e}\Phi M_{th}sin\left(\frac{\pi w}{2\tau}\right), \quad (14)$$

where w represents the width of PM, and g_e represents the effective air gap length.

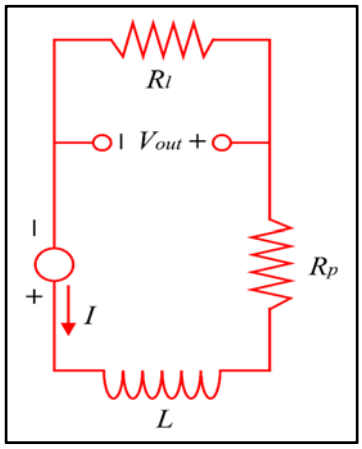

Fig. 5: Equivalent circuit of the LEM

2.1.3 Friction model

The friction of a four-stroke engine was analyzed by Heywood[51]. Friction can be classified into four main parts, namely, crankshaft bearings 10%, accessories 15%, valve train 25%, and piston assembly 50%[51]. However, the friction value in the FPELG is smaller compared with those of conventional ICEs because the crankshaft and other parts connected to the crankshaft are absent in the FPELG. Thus, the friction of the piston assembly and the LEM can be considered the main value of the FPELG's friction force. In order to drive the friction force model, the main equation to calculate the friction force of FPELG can be expressed as

$$F_f = F_{fr} + F_{fl} + F_{fLEM}, \tag{15}$$

where F_f (N) represents the total friction, F_{fr} (N) represents the friction of the right cylinder, F_{fl} (N) represents the friction of the left cylinder, and F_{fLEM} (N) represents the friction of the LEM.

The friction between the mover and stator represents the LEM friction force. When the engine is running stably, the velocity of the piston is almost fixed. Thus, the LEM friction force is assumed to be constant. According to the above details, the final equation to calculate FPELG friction can be written as

$$F_{fr} = \epsilon\left[-Di(V_P)a\sqrt{|V_P|}\right]\left[1 - b\frac{T_l - T_a}{T_a}\right]\left[1 + c \times \frac{P_r(t)}{P_a}\right]\left[\frac{D_b}{D_a}\right], \tag{16}$$

where ϵ (unit: -) represents the scaling factor, a, b, and c (-) are the friction factors, V_P (m/s) represents the velocity of the piston, T_l (°C) represents the temperature of the lubrication oil, D_b (mm) represents the cylinder diameter, D_a represents the cylinder diameter (reference), D_i represents the directional movement, T_a (°C) represents the ambient temperature, P_r (bar) represents the simultaneous gas pressure, and P_a represents the ambient pressure.

3. Methodology of the simulation model

The methodology used to establish the air-driven expander FPE is discussed in this section. Here, the FPELG operation concept may be described as the forces used in the FPLE. The forces are classified into four parts, namely, the force acting on the right piston, the force acting on the left piston, the force of LEM, and the total friction force. Assuming the compressed air is provided to the left chamber then the piston is moved from TDC to BDC. During this movement, the energy is stored in the right chamber. Then, the pressure in the right cylinder pushes back the piston again to the left side. By repeating this process, a resonance movement is generated, and the current is generated by the LEM. In this study, MATLAB/Simulink was used on the basis of a zero-dimensional model to build the FPLE system's model. According to mathematical equations, the model should include the forces that originate from the left and right cylinders (i.e., the air-driven expander), the LEM force, and the friction force. Figure 6 shows the simulation model of the air-driven FPLE built using MATLAB/Simulink. Some assumptions are considered in this model. The parameters such as gas leakage and heat transfer are neglected because of their extremely small values. Based on Newton's second law, the dynamic model is built as shown in Figure 6. It can be seen from the figure the left and right cylinder models are connected to the LEM model. In addition, the system model, including the friction sub-model and control, is developed. Figure 7 shows a detailed dynamic model of the FPLE simulation. While Figure 8 shows a detailed simulation model of the air-driven expander for a cylinder of the engine side, which is similar to the configuration in the other side. Figures 9 shows the LEM model. The simulation model is validated using experimental data. By using this model, the characteristics of the air-driven expander FPLE, such as the piston linear position profile, velocity of the piston, the in-cylinder pressure, and the engine power can be investigated.

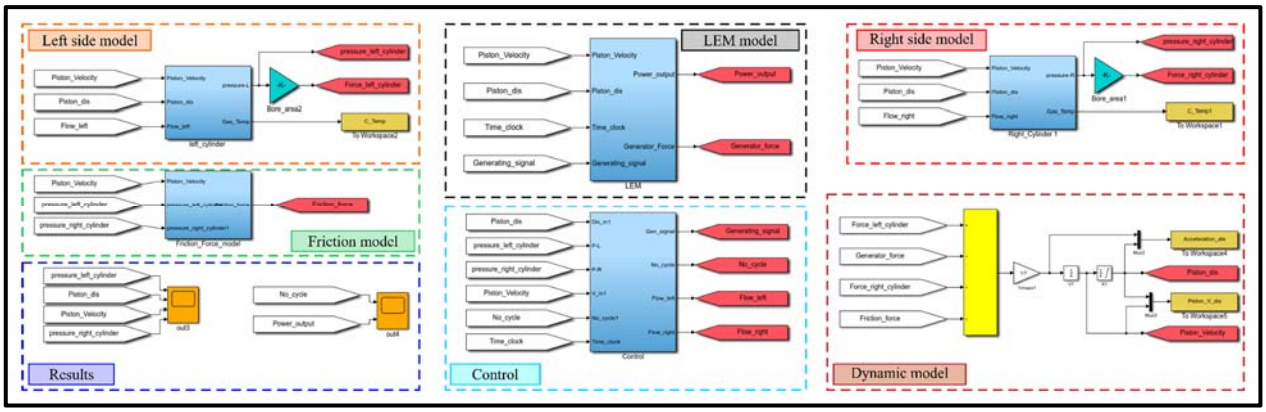

Fig. 6: Detailed simulation model of the air-driven FPLE

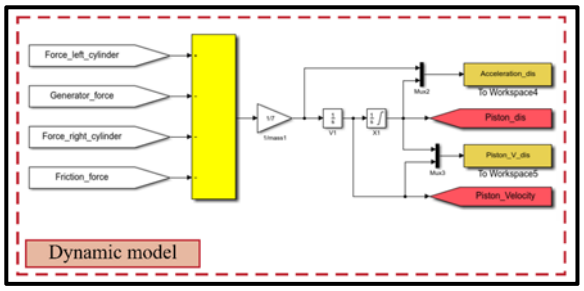

Fig. 7: Detailed dynamic model of the simulation

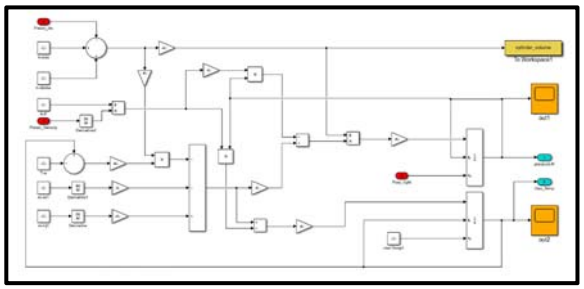

Fig. 8: Detailed engine cylinder model of the simulation

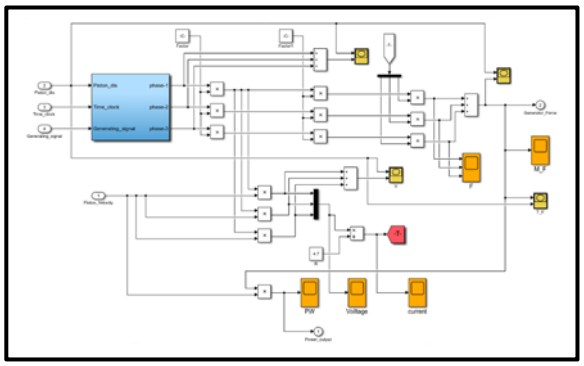

Fig. 9: Detailed LEM model of the simulation

4. Validation

4.1 Experimental setup

In order to validate the simulation model, the experiment was conducted using a rig of the air-driven FPLE prototype in Universiti Teknologi PETRONAS (UTP) at the Centre for Automotive Research and Electrical Mobility (CAREM). Table 1 shows the operating conditions and specifications of the air-driven FPLE for both experimental and simulation models.

Table 1. Parameters and operating conditions of the air-driven FPLE

Parameter	**Value**
Bore of cylinder for both sides	56 mm
Maximum stroke	96 mm
Effective stroke	84 mm
Mass of connecting rod and piston	7 kg
Resistance (external load)	4.8 ohm
Cylinders Number	2
Intake pressure	5 bar
Frequency	13
Cylinder volume	221 cc

Figure 10 shows the configuration of the air-driven FPLE prototype. The prototype is composed of two cylinders, and both cylinders work with compressed air. The compressed air is provided to the cylinders through valves. The LEM is connected between these two air-driven chambers. The main control unit (MCU) is also connected to the prototype for controlling the signals.

Figure 11 shows a diagram of the experimental setup and the control system. Compressed air is supplied to the prototype by using a compressor and a tank. Some accessories, such as sensors, gauges, regulators, connectors, and high-pressure pipes, are provided. The intake pressure value of 5 bar is supplied to the chambers to alternately produce resonance movement. Current is generated from LEM during the resonance movement. In-cylinder pressure, displacement, and power data are collected.

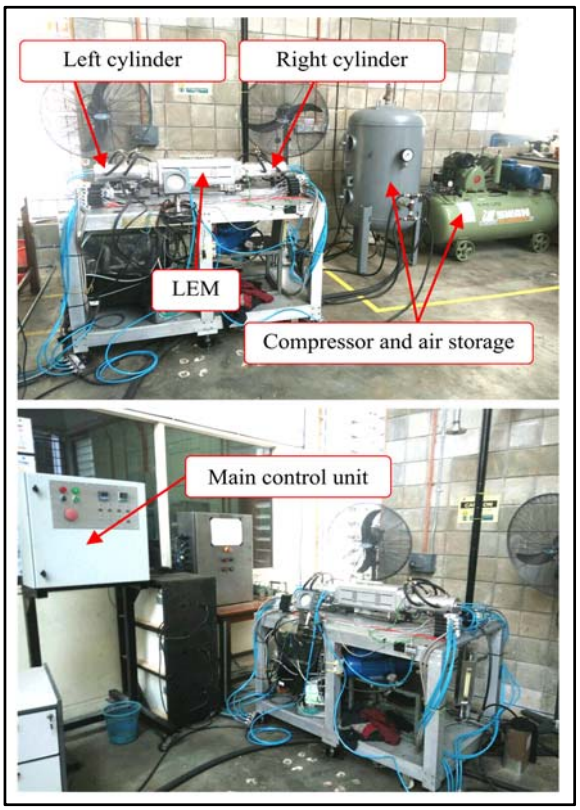

Fig. 10: Configuration of the air-driven FPLE prototype

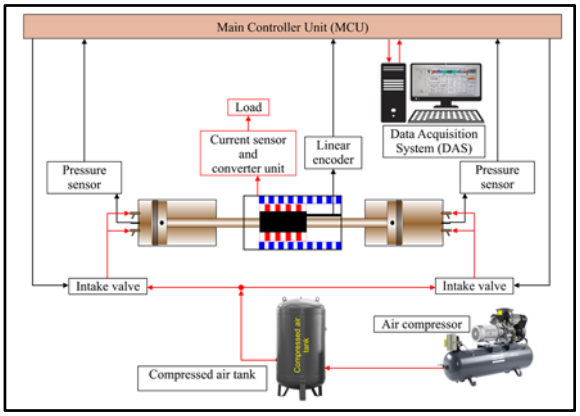

Fig. 11: Diagram of the experimental setup and control system of the air-driven FPLE

4.2 Validation results

A specified set of experimental measures was verified in the experimental tests. After the data collection, the experimental results were analyzed and then compared with the simulation data. The in-cylinder pressure profiles in both simulation and experimental data are illustrated in Figure 12.

The data of five cycles for both simulation and experiment were used for validation. It can be seen from the Figure that the peak pressure in the simulation data was less varied compared with that in the experimental data. In addition, the simulation results of the in-cylinder pressure were higher than the in-cylinder pressure of the experiment. Despite the difference, the simulation result almost corresponds to the experimental data within an acceptable error range. In particular, the maximum difference (error) is less than 10%, as shown in Figure12. However, the errors of most in-cylinder pressure values between the simulation result and the experimental data were less than 5%, thus verifying the validity of the model. Meanwhile, the piston's linear position against time for both simulation and experimental data is illustrated in Figure 13.

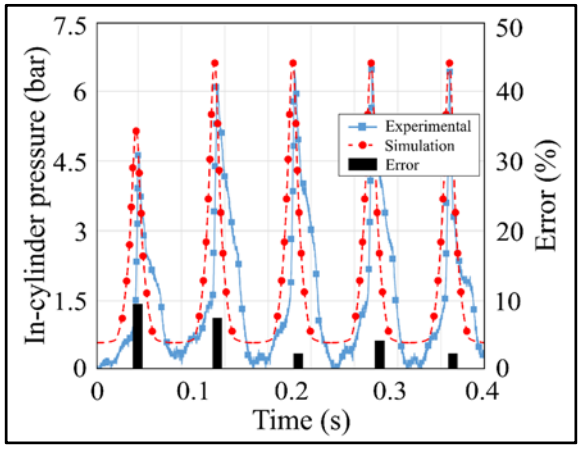

Fig. 12: Comparisons of in-cylinder pressures between experimental data and simulation results with error percentage

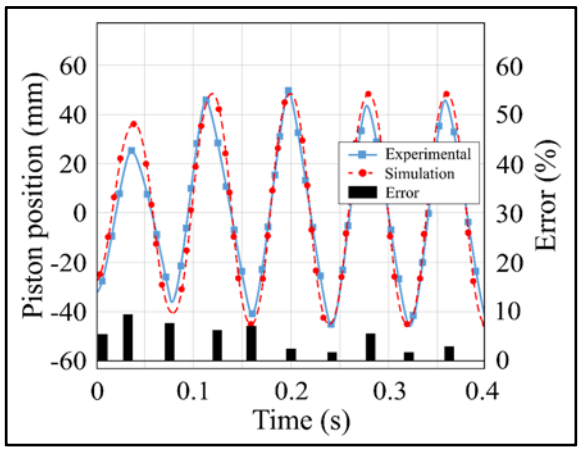

Fig. 13: Comparisons of piston displacement profiles between experimental data and simulation results with error percentage

Some variations can be observed in the experimental data. Thus, the error percentage after comparing the simulation and experimental data was further calculated. As shown in the figure, the errors of most piston displacement values between the simulation result and the experimental data were also less than 5%. However, the maximum error was less than 10%, which is within an acceptable range. These errors can be attributed to the accuracy of instrumentation and sensors used in the experiment. Moreover, the leakage between the piston ring and cylinder wall and certain environmental conditions could have affected the experimental data. Nonetheless, an assumption was considered for the

simulation model of the aforementioned in detail in the modeling section of this study. However, the derived comparison indicates that the model is valid and can be used to predict results for investigating the characteristics of a dual-piston air-driven expander linear generator.

5. Simulation results and discussion

In this study, three different values of intake pressure, i.e., the pressure at 5, 6, and 7 bar were selected for the simulation test. The other parameters of the engine model were set according to the values listed in Table 1. Figure 14 shows the piston displacement profile, piston velocity, and in-cylinder pressure of both sides (i.e., left and right sides) when the intake pressure is set with 5 bar.

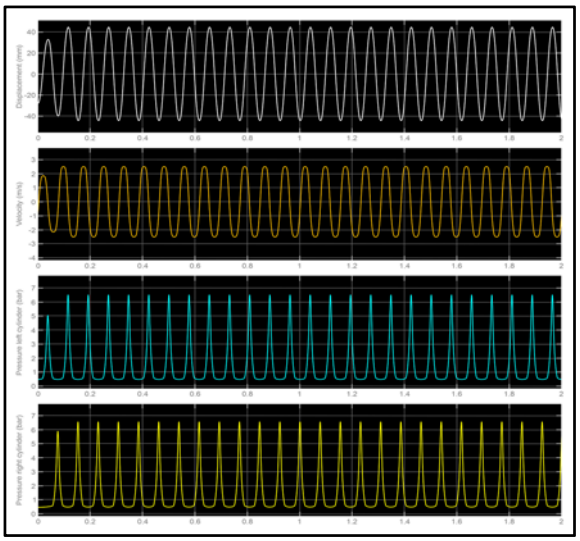

Fig. 14: Simulation results of the piston displacement profile, piston velocity, and in-cylinder pressure of the left and right sides

The maximum piston linear position at TDC and BDC are 44 and -44 mm, respectively. The results of the piston displacement indicate that the engine work with a full stroke, and the piston can reach the right position i.e., if the piston displacement is more than this value the piston may hit the cylinder head, and if less than this value will produce less power. In addition, the frequency (13 Hz) can be clearly calculated from the displacement profile. The piston velocity profile is shown in Figure 14. The maximum value of piston velocity is achieved at 2.5 m/s. While the in-cylinder pressure in both sides increases to approximately 6.5 bar when the engine model has an intake pressure of 5 bar.

The results are further analyzed by determining the relation between piston velocity and displacement (Figure 15). It can be seen from the figure that the piston achieves the maximum velocity when it approaches the middle of the stroke in the plot, and the value decreases dramatically at TDC or BDC. This finding is similar to those of previous studies[5,44]. The highest piston velocity was approximately 2.5 m/s at the intake pressure of 5 bar. Then, the piston velocity increased further near TDC and BDC, followed by a significant decrease. This trend differs from that of the crankshaft engine in which the piston velocity is slower around TDC and BDC because it is restricted by the crankshaft mechanism or it follows the crankshaft path[52].

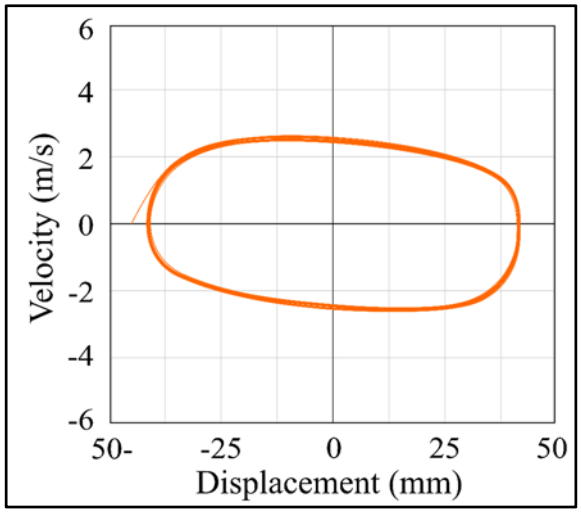

Fig. 15: Profile of piston velocity against piston displacement

The plot of in-cylinder pressure against time for both cylinders (left and right cylinders) is shown in Figure 16. It can be seen from the figure that the pressure increased gradually from 5 bar (intake pressure) to approximately 6.5 bar, but the increase was dependent on the energy saved by the gas spring at each stroke. However, a few other parameters are also affecting on the in-cylinder pressure such as the duration time were used for the intake valve (open/close timing).

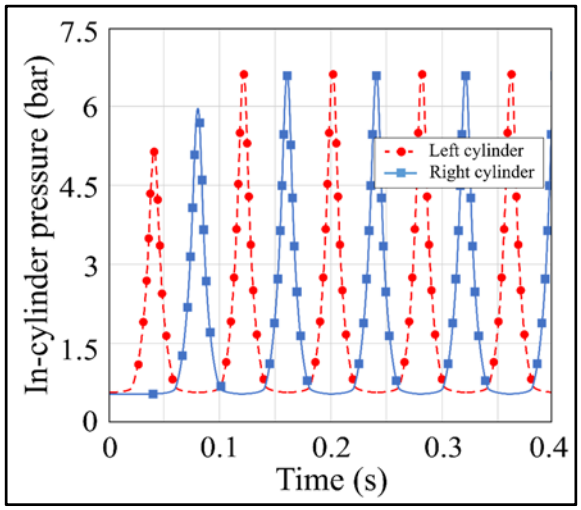

Fig. 16: Profile of in-cylinder pressure against time for the left and right cylinders

The results further indicate that peak pressure is produced alternatingly. In particular, the pressure

decreased to a minimum value at the right cylinder when the pressure reached the maximum value in the left cylinder and vice versa. This trend suggests that the expansion stroke occurred in the right cylinder when the compression stroke occurred at the left cylinder; as a result, the maximum in-cylinder pressure was recorded at the TDC and BDC. Consequently, the in-cylinder pressure was used as the main parameter to evaluate the power output of the FPLE. High in-cylinder pressure corresponds to high power output. However, some other parameters (e.g., piston displacement between TDC and BDC) could negatively affect the high in-cylinder pressure. Thus, stroke length was affected; in particular, its value decreased.

The characteristics of the air-driven expander FPELG was further investigated by conducting a simulation test. Different intake pressures (5, 6, and 7 bar) were considered. Figure 17 shows the influence of the different intake pressures on the in-cylinder pressure. The findings indicate that in-cylinder pressure is directly related to intake pressure. When the intake pressure is increased, the in-cylinder pressure also increases. The in-cylinder pressure is increased by approximately 16% when the intake pressure is increased from 5 to 6 bar. While the in-cylinder pressure is increased by approximately 21.7% when the intake pressure is increased from 6 to 7 bar. This trend indicates that in-cylinder pressure has a nonlinear relationship with intake pressure. From the figure, the maximum in-cylinder pressure can be obtained when the intake pressure is at the maximum. However, the optimal intake pressure also depends on certain parameters, such as engine design, valve opening time, and load. Overall, the findings imply that engine performance can be improved when high intake pressure is supplied to the system.

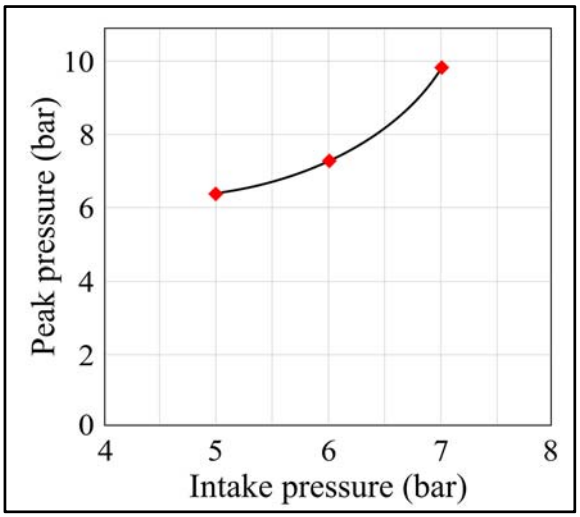

Fig. 17: Effect of different intake pressures on in-cylinder pressure

For the piston velocity, Figure 18 illustrates the influence of intake pressure on piston velocity. According to the simulation results, piston velocity is directly proportional with intake pressure, and the relationship is linear. From the figure can be seen the piston velocity is low at the intake pressure of 5 bar, and it is high at 7 bar. As combustion does not occur in this type of engine, thus, the cylinder working as a gas spring. Thus, a possible reason for the increase in piston velocity is the energy stored by each cylinder, which increases when the pressure increases under the same cylinder volume and other conditions. The induced voltage is high when the engine works at the maximum piston velocity. This finding indicates that output power can be increased when the piston velocity is maximized. Can be concluded that the piston velocity is increased by approximately 12.3% when the intake pressure is increased by 1 bar.

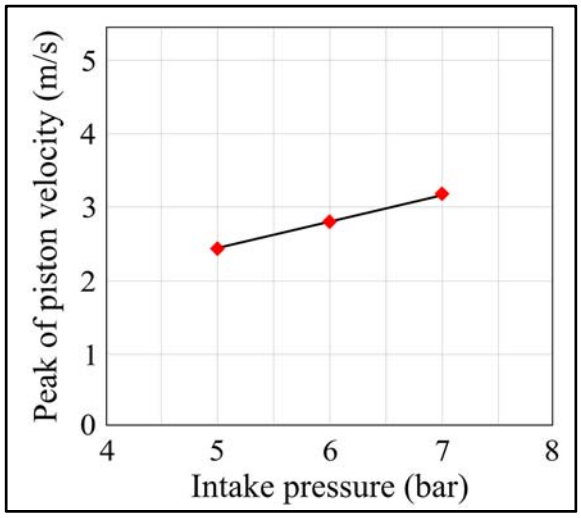

Fig. 18: Effect of different intake pressures on piston velocity

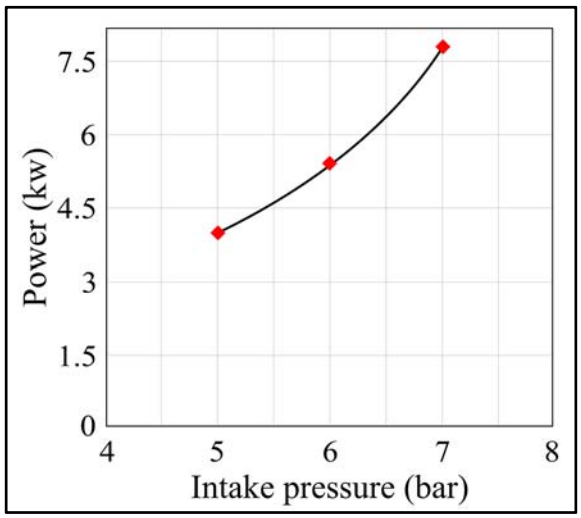

Fig. 19: Effect of different intake pressure on the engine power

The simulation model can predict the results of the engine power. Figure 19 shows the effect of intake pressure on engine power. From the figure can be seen that the power is increased when the intake pressure is increased. In addition, can be observed that the increase in

power is not linearly proportional to intake pressure. A high engine power (7.5 kW) is observed at the intake pressure of 7 bar. The engine power increases by approximately 26.5% when the intake pressure increases from 5 to 6 bar. While the engine power increases by approximately 30.6% when the intake pressure increases from 6 to 7 bar. However, engine power does not refer to the output power because there are some losses that occur in the conversion of energy by LEM. These losses pertain to LEM friction force, heat transfer, cogging force, the number of the stator core, and design factors. All these parameters affect output power. Thus, further study is needed to investigate the output power of air-driven expander FPELG. In addition, the efficiency of air-driven expander FPELGs under different intake pressures should be determined.

In summary, an air-driven expander FPELG model is proposed in this study. As the simulation model can successfully predicted the results, it can also be used to analyze the characteristics of engines. According to the simulation results, can be indicated that the intake pressure significantly affects the performance of the air-driven expander FPELG. In addition, the optimal intake pressure is required to enhance engine performance.

6. Conclusion

This study established a numerical model of the dual-piston air-driven FPLE based on the FPELG concept. MATLAB/Simulink was used to build the zero-dimensional numerical model. Experimental data were used to validate the simulation results. The simulation results were in good agreement with experimental data for both in-cylinder pressure and displacement profile. In addition, the measured error was within the acceptable range of less than 10%, indicating that the model can successfully predict the results. The effect of intake pressure on displacement profile, in-cylinder pressure, piston velocity, and engine power were also investigated in this study.

The simulation results also showed that intake pressure plays a significant role in FPLE engine performance. The in-cylinder pressure was increased by approximately 16% when the intake pressure increased from 5 to 6 bar. While the in-cylinder pressure was increased by approximately 21.7% when the intake pressure increased from 6 to 7 bar. As for piston velocity, a linear relationship was observed between intake pressure and piston velocity, and the increase was approximately 12.3% when the intake pressure was increased by 1 bar. Moreover, engine power was increased by approximately 26.5% when the intake pressure was increased from 5 to 6 bar. While the engine power was increased by approximately 30.6% when the intake pressure was increased from 6 to 7 bar. This study has presented a fundamental analysis of FPLE engines. Further research is required to explore in detail the optimal value of intake pressure.

Acknowledgements

The authors gratefully acknowledge the support of this work by the Centre for Automobile and Electric Mobility (CAREM), Universiti Teknologi PETRONAS, 32610 Seri Iskandar, Perak Darul Ridzuan, Malaysia Perak, Malaysia.

Funding: This work was supported by the Petroleum Research Fund (PRF) Grant (grant numbers 0153AB-A34); Centre for Automobile and Electric Mobility (CAREM), Universiti Teknologi PETRONAS.

Nomenclature

FPLE	Free piston linear expander
LEM	Linear electric machine
FPELG	Free piston engine linear generator
ICE	Internal combustion engines
TDC	Top dead center
BDC	Bottom dead center
PM	Permanent magnets
m	Mover assembly mass (kg)
x	Instantaneous piston displacement (m)
t	time (s)
F_l	Force acting on piston in the left cylinder (N)
F_r	Force acting on the piston in the right cylinder (N)
F_f	Friction force (N)
F_{LEM}	LEM force (N)
E_s	Stored energy (J)
V_T	Instantaneous volume when the piston's position is at TDC (m^3)
V_B	Instantaneous volume when the piston's position is at BDC (m^3)
P_{ins}	Instantaneous gas pressure in the cylinder (bar)
P_0	Initial gas pressure in the cylinder (bar)
V	Instantaneous working volume(m^3)
E_c	Energy of compression (J)
P	In-cylinder gas pressure (bar)
C	Constant
P_r	Gas pressure in the right cylinder (bar)
m_{inj}	Mass of injected gas
m_{ex}	Mass of exhausted gas
A_T	Total area of heat transfer (m^2)
T	Temperature of the chamber (K)
T_w	Temperature of cylinder wall (K)
h_m	Minimum distance (the distance from TDC to the head of the cylinder) (m)

D_b	Cylinder's bore diameter (m)
N	Coil turns number
e	Induced voltage (V)
I	Instantaneous current (I)
R_p	Phase-winding resistance
R_l	Load resistance (ohm)
M_{th}	PM thickness
L_c	Coil length that cuts the magnetic lines (m)
F_f	Total friction (N)
F_{fr}	Friction of the right cylinder (N)
F_{fl}	Friction of the left cylinder (N)
F_{fLEM}	Friction of the LEM (N)
a, b, c	Friction factors
V_P	Velocity of the piston (m/s)
T_l	Temperature of the lubrication oil (°C)
T_a	Ambient temperature (°C)
D_b	Cylinder diameter (m)
D_a	Cylinder diameter (reference)
D_i	Directional movement
P_r	Simultaneous gas pressure (bar)
P_a	Ambient pressure (bar)

Greek symbols

γ	Polytropic exponent
μ_{inj}	Injected mass enthalpy
μ_{ex}	Exhausted mass enthalpy
ρ	Heat transfer coefficient
Φ	Flux number
ε	Instantaneous voltage (V)
φ	Vacuum permeability
ϵ	Scaling factor

References

1) M. Al-Ghriybah, M. Fadhli Zulkafli, D. Hissein Didane, and S. Mohd, "The effect of spacing between inner blades on the performance of the savonius wind turbine," *Sustain. Energy Technol. Assessments*, **43** (*January*) 100988 (2021). doi:10.1016/j.seta.2020.100988.
2) M. Al-Ghriybah, M.F. Zulkafli, D.H. Didane, and S. Mohd, "The effect of inner blade position on the performance of the savonius rotor," *Sustain. Energy Technol. Assessments*, **36** (*September*) (2019). doi:10.1016/j.seta.2019.100534.
3) A. Habibie, M. Hisjam, W. Sutopo, and M. Nizam, "Sustainability evaluation of internal combustion engine motorcycle to electric motorcycle conversion," *Evergreen*, **8** (*2*) 469–476 (2021). doi:10.5109/4480731.
4) R. Mikalsen, and A.P. Roskilly, "A review of free-piston engine history and applications," *Appl. Therm. Eng.*, **27** (*14–15*) 2339–2352 (2007). doi:10.1016/j.applthermaleng.2007.03.015.
5) N.B. Hung, and O. Lim, "A review of free-piston linear engines," *Appl. Energy*, **178** 78–97 (2016).
6) A.T. Raheem, A.R. A. Aziz, S. A. Zulkifli, A.T. Rahem, and W.B. Ayandotun, "A review of free piston engine control literature—taxonomy and techniques," *Alexandria Eng. J.*, **61** (*10*) 7877–7916 (2022). doi:10.1016/j.aej.2022.01.027.
7) R.P. Pescara, "Motor compressor apparatus," *United States Pat. Off.*, **11** (*6*) 371–374 (1928). http://stacks.iop.org/1402-4896/11/i=6/a=006?key=crossref.7d00a8ac08fc7c00b62722b967635c86.
8) R.P. Pescara, "Motor compressor of the free piston type," *United States Pat. Off.*, (1941).
9) A.T. Raheem, A.R.A. Aziz, S.A. Zulkifli, M.B. Baharom, A.T. Rahem, and W.B. Ayandotun, "Optimisation of operating parameters on the performance characteristics of a free piston engine linear generator fuelled by cng–h2 blends using the response surface methodology (rsm)," *Int. J. Hydrogen Energy*, **47** (*3*) 1996–2016 (2022). doi:10.1016/j.ijhydene.2021.10.125.
10) B. Jia, Z. Zuo, G. Tian, H. Feng, and A.P. Roskilly, "Development and validation of a free-piston engine generator numerical model," *Energy Convers. Manag.*, **91** 333–341 (2015).
11) H. Kosaka, T. Akita, K. Moriya, S. Goto, Y. Hotta, T. Umeno, and K. Nakakita, "Development of free piston engine linear generator system part 1-investigation of fundamental characteristics," SAE Technical Paper, 2014.
12) X. Wang, F. Chen, R. Zhu, G. Yang, and C. Zhang, "A review of the design and control of free-piston linear generator," *Energies*, **11** (*8*) 2179 (2018).
13) R. Mikalsen, and A.P. Roskilly, "The control of a free-piston engine generator. part 1: fundamental analyses," *Appl. Energy*, **87** (*4*) 1273–1280 (2010).
14) R. Mikalsen, E. Jones, and A.P. Roskilly, "Predictive piston motion control in a free-piston internal combustion engine," *Appl. Energy*, **87** (*5*) 1722–1728 (2010).
15) C. Guo, Z. Zuo, H. Feng, B. Jia, and T. Roskilly, "Review of recent advances of free-piston internal combustion engine linear generator," *Appl. Energy*, **269** 115084 (2020).
16) R. Mikalsen, and A.P. Roskilly, "Performance simulation of a spark ignited free-piston engine generator," *Appl. Therm. Eng.*, **28** (*14–15*) 1726–1733 (2008).
17) Y. Wang, L. Chen, B. Jia, and A.P. Roskilly, "Experimental study of the operation characteristics of an air-driven free-piston linear expander," *Appl. Energy*, **195** 93–99 (2017).
18) A.T. Raheem, A.R.A. Aziz, S.A. Zulkifli, W.B.

Ayandotun, E.Z. Zainal, and S.M. Elfakki, "Experimental Analysis for the Influence of Ignition Time on Combustion Characteristics of a Free Piston Engine Linear Generator," in: J. Phys. Conf. Ser., IOP Publishing, 2021: p. 12051. doi:10.1088/1742-6596/1793/1/012051.

19) Y. Zhou, A. Sofianopoulos, B. Lawler, and S. Mamalis, "Advanced combustion free-piston engines: a comprehensive review," *Int. J. Engine Res.*, **21** (*7*) 1205–1230 (2020). doi:10.1177/1468087418800612.
20) W.B. Ayandotun, A.R.A. Aziz, Z.A.B.A. Karim, S.E. Mohammed, A.T. Raheem, and M.A. Ismael, "Investigation on the combustion and performance characteristics of a di free piston linear generator engine fuelled with cng-co2 blend," *Appl. Therm. Eng.*, 117441 (2021).
21) R. Mikalsen, and A.P. Roskilly, "The design and simulation of a two-stroke free-piston compression ignition engine for electrical power generation," *Appl. Therm. Eng.*, **28** (*5–6*) 589–600 (2008).
22) Z. Zhang, H. Feng, B. Jia, Z. Zuo, A. Smallbone, and A.P. Roskilly, "Effect of the stroke-to-bore ratio on the performance of a dual-piston free piston engine generator," *Appl. Therm. Eng.*, **185** 116456 (2021).
23) S.A. Zulkifli, M.N. Karsiti, and A.R.A. Aziz, "Starting of a free-piston linear engine-generator by mechanical resonance and rectangular current commutation," in: 2008 IEEE Veh. Power Propuls. Conf., IEEE, 2008: pp. 1–7.
24) Q. Li, J. Xiao, and Z. Huang, "Simulation of a two-stroke free-piston engine for electrical power generation," *Energy & Fuels*, **22** (*5*) 3443–3449 (2008).
25) H.N. Ba, O. Lim, and N. Iida, "Simulation study of si-hcci transition in a two-stroke free piston engine fuelled with propane," *SAE Tech. Pap.*, **1** (2014).
26) L. Wu, H. Feng, Z. Zhang, Z. Tang, B. Jia, and X. Yan, "Research on starting process and control strategy of opposed-piston free-piston engine generator _ simulation and test results," *Energy Reports*, **7** 4977–4987 (2021).
27) Y. Zhu, Z. Tang, and H. Feng, "Simulation of the in-cylinder working process of an Opposed-Piston Free-Piston Linear Generator," in: IOP Conf. Ser. Mater. Sci. Eng., IOP Publishing, 2019: p. 12093.
28) N.B. Hung, O. Lim, and N. Iida, "The effects of key parameters on the transition from si combustion to hcci combustion in a two-stroke free piston linear engine," *Appl. Energy*, **137** 385–401 (2015).
29) Z. Zhao, F. Zhang, Y. Huang, C. Zhao, and F. Guo, "An experimental study of the hydraulic free piston engine," *Appl. Energy*, **99** 226–233 (2012).
30) J. Hu, W. Wu, S. Yuan, and C. Jing, "Fuel combustion under asymmetric piston motion: tested results," *Energy*, **55** 209–215 (2013).
31) E.Z.Z. Abidin, A. A Ibrahim, A.R. A Aziz, and S. A Zulkifl, "Investigation of starting behaviour of a free-piston linear generator," *J. Appl. Sci.*, **12** (*24*) 2592–2597 (2012).
32) B. Jia, G. Tian, H. Feng, Z. Zuo, and A.P. Roskilly, "An experimental investigation into the starting process of free-piston engine generator," *Appl. Energy*, **157** 798–804 (2015).
33) Y. Zhu, Y. Wang, X. Zhen, S. Guan, J. Wang, Y. Wu, Y. Chen, and S. Yin, "The control of an opposed hydraulic free piston engine," *Appl. Energy*, **126** 213–220 (2014).
34) R. Mikalsen, and A.P. Roskilly, "A computational study of free-piston diesel engine combustion," *Appl. Energy*, **86** (*7–8*) 1136–1143 (2009).
35) S.S. Goldsborough, and P. Van Blarigan, "A numerical study of a free piston ic engine operating on homogeneous charge compression ignition combustion," *SAE Trans.*, 959–972 (1999).
36) C.M. Atkinson, S. Petreanu, N.N. Clark, R.J. Atkinson, T.I. McDaniel, S. Nandkumar, and P. Famouri, "Numerical simulation of a two-stroke linear engine-alternator combination," *SAE Trans.*, 1416–1430 (1999).
37) M. Bade, N.N. Clark, T. Musho, and P. Famouri, "Piston rings friction comparison in a free piston and conventional crankshaft engines," in: Intern. Combust. Engine Div. Fall Tech. Conf., American Society of Mechanical Engineers, 2018: p. V002T07A012.
38) M. Bade, N.N. Clark, P. Famouri, and P. Guggilapu, "Translator dynamics and performance comparison on one and two cylinder free piston engines," in: ASME Int. Mech. Eng. Congr. Expo., American Society of Mechanical Engineers, 2018: p. V06AT08A039.
39) H. Feng, Z. Zhang, B. Jia, Z. Zuo, A. Smallbone, and A.P. Roskilly, "Investigation of the optimum operating condition of a dual piston type free piston engine generator during engine cold start-up process," *Appl. Therm. Eng.*, **182** 116124 (2021).
40) M.P. Hekkert, F.H.J.F. Hendriks, A.P.C. Faaij, and M.L. Neelis, "Natural gas as an alternative to crude oil in automotive fuel chains well-to-wheel analysis and transition strategy development," *Energy Policy*, **33** (*5*) 579–594 (2005).
41) A. Kowalewicz, and M. Wojtyniak, "Alternative fuels and their application to combustion engines," *Proc. Inst. Mech. Eng. Part D J. Automob. Eng.*, **219** (*1*) 103–125 (2005).
42) M.A. Ismael, A.R.A. Aziz, S.E. Mohammed, E.Z. Zainal A, M.B. Baharom, A.T. Raheem, W.B. Ayandotun, F.I. Harith, and I. Khazaimah, "Experimental study on combustion stability and performance of hydrogen-enriched compressed natural gas of a free-piston linear generator," *Int. J. Hydrogen Energy*, **46** (*79*) 39536–39547 (2021). doi:10.1016/j.ijhydene.2021.09.156.

43) A. Cernat, C. Pana, N. Negurescu, G. Lazaroiu, C. Nutu, and D. Fuiorescu, "Hydrogen—an alternative fuel for automotive diesel engines used in transportation," *Sustainability*, **12** (*22*) 9321 (2020).
44) F. Huang, and W. Kong, "Effect of hydrogen addition on the operating characteristics of a free piston linear engine," *Int. J. Hydrogen Energy*, **45** (*30*) 15402–15413 (2020).
45) M.A. Ismael, A.R.A. Aziz, S.E. Mohammed, W.B. Ayandotun, M.B. Baharom, M.S. Sallehudin, A.R.T. Anwerudin, and M.M. Masri, "Investigation on free-piston motion and power generation of a dual-piston air-driven expander linear generator," *Energy Reports*, **7** 2388–2397 (2021).
46) H. Amiruddin, W.M.F.W. Mahmood, S. Abdullah, and M.R.A. Mansor, "CNGDI engine performance using a vaned diffuser turbocharger compressor with varying injection timings," *Evergreen*, **8** (*2*) 414–420 (2021). doi:10.5109/4480723.
47) M. Muslimm, M.I. Alhamid, and B. Ismoyo, "Analysis of the scroll compressor changing into an expander for small scale power plants using an organic rankine cycle system," *Evergreen*, **7** (*4*) 615–620 (2020).
48) F. Adian, and B. Sugiarto, "The optimization of the relationship between octane number of gasoline-ethanol blend fuels in various settings of the engine control module," *Evergreen*, **7** (*4*) 587–592 (2020). doi:10.5109/4150510.
49) F. Nehad Abed, A. Abdullah Hamad, and A. Bin Sapit, "The effect analysis for the nano powder dielectric processing of ti-6242 alloy is performed on wire cut-electric discharge," *Mater. Today Proc.*, (*xxxx*) (2020). doi:10.1016/j.matpr.2020.09.368.
50) F. Kock, and F. Rinderknecht, "A high efficient energy converter for a hybrid vehicle concept-gas spring focused," *Tagungsband EVER 12*, (2012).
51) J.B. Heywood, "Internal combustion engine fundamentals," McGraw-Hill Education, 2018.
52) C. Guo, H. Feng, B. Jia, Z. Zuo, Y. Guo, and T. Roskilly, "Research on the operation characteristics of a free-piston linear generator: numerical model and experimental results," *Energy Convers. Manag.*, **131** 32–43 (2017).